Interfacial shape and contact-angle measurement of transparent samples with confocal interference microscopy

David G. Fischer

National Center for Microgravity Research on Fluids and Combustion, NASA Glenn Research Center, MS 110-3, 21000 Brookpark Road, Cleveland, Ohio 44135

Ben Ovryn

National Center for Microgravity Research on Fluids and Combustion, NASA Glenn Research Center, MS 110-3, 21000 Brookpark Road, Cleveland, Ohio 44135, and
Department of Mechanical and Aerospace Engineering, Case Western Reserve University, Cleveland, Ohio 44106

Received November 8, 1999

A model has been developed that predicts the effective optical path through a thick, refractive specimen on a reflective substrate, as measured with a scanning confocal interference microscope equipped with a high-numerical-aperture objective. Assuming that the effective pinhole of the confocal microscope has an infinitesimal diameter, only one ray in the illumination bundle (the magic ray) contributes to the differential optical path length (OPL). A pinhole with finite diameter, however, allows rays within a small angular cone centered on the magic ray to contribute to the OPL. The model was incorporated into an iterative algorithm that allows the measured phase to be corrected for refractive errors by use of an *a priori* estimate of the sample profile. The algorithm was validated with a reflected-light microscope equipped with a phase-shifting laser-feedback interferometer to measure the interface shape and the 68° contact angle of a silicone-oil drop on a coated silicon wafer. © 2000 Optical Society of America

OCIS codes: 120.3180, 170.1790, 180.3170, 120.3940, 120.2830.

The determination of the static or dynamic shape of a transparent sample on a solid substrate is a common goal of many research disciplines. For example, a detailed understanding of dynamic wetting phenomena requires high transverse- and axial-resolution measurements of the topography of a fluid's surface.[1] Industrial applications that depend on the mass transport of a viscous liquid over a substrate are ubiquitous: dip coating of sheet metals, gravity drainage of paints, spin coating of surface layers on silicon substrates, coating of inks on paper, and the production of microlenses. In the last category, regardless of the production method (e.g, polymer melting,[2] thin-film deposition,[3] microjetting of thermoplastics resins or polymers,[4] multilevel etching[5]), careful monitoring of the ultimate shape is required if one is to achieve a lens with as high a numerical apeture (NA) as possible. On a smaller scale, the understanding of the interaction of proteins with smooth and structured surfaces is an area of active research that requires the precise measurement of the deformation of the protein (e.g., a membrane) as it contacts the surface.[6–8]

Although optical measurements with low spatial resolution have been used to measure both dynamic and static wetting properties (e.g., contact lines and equilibrium contact angles),[9] these methods are currently being augmented by high-NA microscope techniques, and the highest accuracy is attained when these techniques are combined with interferometry.[6–8,10] When a high-NA interference microscope is used to determine the optical path length (OPL) through a thick, curved refractive sample on a substrate, the precise determination of the interference phase of the rays in the incident cone is not a trivial matter. Fortunately, as we show below, the use of a confocal interference microscope allows the unambiguous determination of the OPL in these specimens.

We have developed a scalar, geometrical-optics-based model to determine the OPL through a thick, curved, transparent specimen that is in contact with a substrate from data obtained with a high-NA reflected-light scanning confocal interference microscope. To correct the OPL measurement for the significant refraction introduced by such a sample we incorporated the model into an iterative algorithm that utilizes an *a priori* estimate of the shape of the sample (i.e., the refractive-index profile). Although it is applicable to any surface shape, we demonstrate the essence of the model and experimentally confirm its applicability to a spherical surface shape; this restriction is nevertheless representative of a large class of samples.

Figure 1 shows the interaction of a convergent wave front from a 0.8-NA objective as it is scanned (from left to right) across a transparent spherically shaped 36-μm-diameter sample that forms a 68° contact angle on a substrate (the objective NA and the diameter of the sample correspond to the parameters used in our experimental measurements). We assume that the substrate is microscopically smooth and that the focus of the microscope is held fixed such that the fringes with the highest visibility are localized on the substrate in a region outside the drop. Figure 1(a) shows that the rays in the incident cone first interact with the sample when the scan location is significantly outside the sample (dotted lines). For scan positions outside the drop, the majority of the incident rays are reflected from the substrate and follow paths that are coincident with the incident rays. Fewer rays

0146-9592/00/070478-03$15.00/0

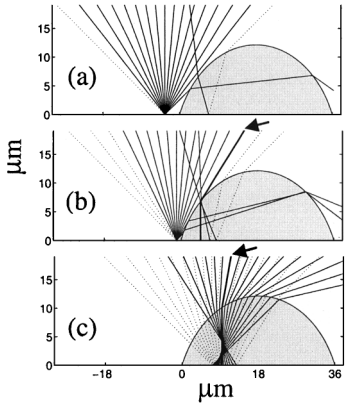

Fig. 1. Ray traces when a high-NA beam is scanned from the left into a spherical drop. (a) $x_S = -4.55\ \mu$m, (b) $x_c = -2.30\ \mu$m, (c) $x_S = 7.51\ \mu$m. The two rays shown by the arrows in (b) and (c) represent magic rays, which after reflection from the substrate follow paths that are coincident with ray paths in the incident cone.

follow paths through the sample and are collected by the objective, but these rays are not coincident with any of the incident rays and ultimately do not make it through the pinhole. When the scan position is sufficiently close to the edge of the drop, however, there is a single ray [arrow in Fig. 1(b)] that upon refraction by the sample and reflection from the substrate is coincident with an incident ray. For scan positions inside the drop [Fig. 1(c)], there is likewise one and only one ray with a path through the sample that is coincident with a ray in the incident cone; we refer to this as the magic ray. As shown in Figs. 1(b) and 1(c), the magic ray is the ray that is refracted at the air–drop interface such that it is normal to the substrate.

The exciting property of the magic ray is that, after refraction by the sample, it appears to originate from a virtual source on the substrate corresponding to the scan position. Because the focal plane is coincident with the substrate surface (in the absence of the sample) the magic ray, together with the rays reflected directly from the substrate, are the only rays that will be transmitted through the infinitesimal-diameter pinhole of a perfect confocal microscope.

Figure 2 shows the optical path of the magic ray when the transverse scan position is located at x_S. After refraction, the ray is reflected by the substrate at point x_R. The phase difference between the magic ray and a ray that would be reflected from the substrate in the absence of the sample can be written as

$$\phi(x_S) = (4\pi/\lambda)\{nh(x_R) - [h(x_R)^2 + (x_S - x_R)^2]^{1/2}\}, \tag{1}$$

where $h(x_R)$ and n are the height (i.e., the normalized OPL) and the refractive index of the sample, respectively, and λ is the wavelength. The height is determined by solution of Eq. (1), with the current (initial) estimate of the sample shape used to calculate the magic-ray location, x_R, corresponding to each scan position x_S. This method is subsequently iterated by use of perturbations in the radius and the contact angle until there is minimal error between the corrected data and the predicted shape.

To validate the algorithm we measured the interface shape of a small drop of fluid that formed a nonzero equilibrium contact angle on a coated substrate, using a confocal interference microscope. This experimental confirmation is motivated by the pioneering work of Thomas Young and Lord Rayleigh; we refer not to their accomplishments in optics but rather to their contributions to the understanding of capillarity.[11,12] A numerical solution for the equilibrium shape of a sessile drop on a clean, smooth substrate (a problem first addressed by Young) predicts the shape of both spherical and nonspherical drops.[13] An analytical solution to an identical problem, the shape of the meniscus in a right-circular capillary tube, provides the height of the meniscus (or drop) as a function of the radial distance from the center of the cylinder (or drop).[14] Provided that the effect of gravitational forces is small compared with the effect of surface tension, (e.g., the Bond number $B = \rho g a^2/\sigma \ll 1$, where ρ is the density, σ is the surface tension, and a is the contact radius of the drop), the shape of the meniscus (or sessile drop) is a spherical segment given by

$$f(r) = \sec(\theta)\{1 - [1 - r^2\cos^2(\theta)]^{1/2}\}, \tag{2}$$

where $f(r)$ is the height of the meniscus as a function of the distance r from the center of the cylinder; we have made both parameters dimensionless by dividing them by the contact radius of the drop. Note that the contact angle θ of the sessile drop (Fig. 2) is the complement of the contact angle for the right-circular cylinder.

A small drop of viscous (60,000 -cS) silicone oil (PDMS; GE Silicones), with a refractive index $n = 1.44$, was deposited on a coated single-crystal silicon wafer; the wafer was cleaned with toluene before being dipped in a fluorinated barrier coat (FC-723; 3M, Inc.).[10] Figure 3 shows a two-dimensional phase image, which we obtained by slowly translating the substrate in a plane transverse to the optical axis of a phase-shifting laser-feedback interference microscope equipped with a 50×/0.8-NA objective.[15] The inset (b) of Fig. 3 shows the phase before unwrapping of the data, at the position delineated in the two-dimensional scan. In addition to the phase information, there is a corresponding visibility image [inset (a) of Fig. 3].[10,15] From the visibility data, the contact radius of the drop was estimated to be 18 μm. Because the Bond number of the drop ($\rho = 980$ kg/m^3, $\sigma = 21.5$ mN/m) was approximately equal to 0.1, the shape of the drop is predicted

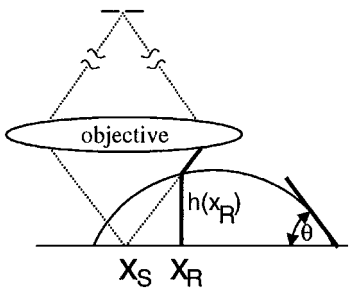

Fig. 2. Optical path of the magic ray for the transverse scan position x_S. The scan position is the point that is conjugate to the pinhole of the confocal microscope.

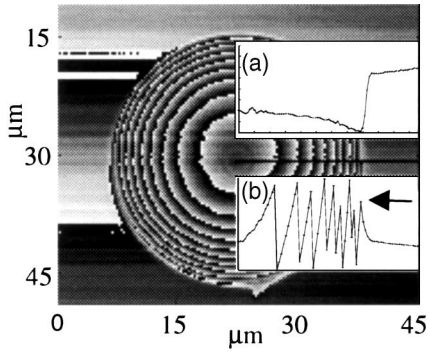

Fig. 3. Two-dimensional phase image before the data were unwrapped. The visibility and the phase along the delineated region are shown in insets (a) and (b), respectively. Only those data points to the left of the arrow in (b) were unwrapped and used for the fit in Fig. 4. The maximum of the visibility was 0.3.

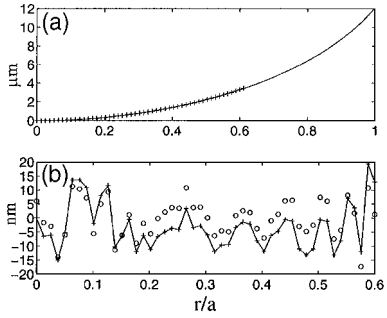

Fig. 4. (a) Superposition of (solid curve) the predicted shape of the fluid drop and (+) the measured shape after correction of the data by use of the magic-ray model. The difference between the two is shown in (b) (+). Also shown is (○) the difference between the corrected data and a high-order polynomial fit to the data. The abscissa is normalized by the contact radius of the drop.

by Eq. (2). The equilibrium contact angle of this drop on the coated substrate as stated in the literature is $\theta = 68°$.[16]

Figure 4(a) shows the measured interface shape (i.e, the corrected data) as a function of normalized scan position from the center of the drop. The interface shape is plotted as a differential height with respect to the apex of the drop so that it will correspond to the case of a right-circular cylinder. Also shown is the interface shape of a spherical drop of 18 μm and $\theta = 68°$ from Eq. (2); the difference between these two is shown in Fig. 4(b). Perturbations in the contact angle as small as 0.02° produce systematic changes in the difference plot and the associated error metric. The accuracy of the algorithm is assessed by comparison of the difference plot with the residual of a high-order polynomial fit to the corrected data.

To mitigate the effect of aliasing of the phase data, which occurs near the edge of the drop, we did not use the pixels to the right of the arrow in Fig. 3(b) in the reconstruction. The exclusion of these pixels also avoids complications due to diffraction near the drop edge.

The error plot shown in Fig. 4(b) indicates that the model used to interpret the OPL through a refractive specimen is correct. To obtain this agreement, however, we had to relax our initial representation of the laser-feedback interference microscope as a perfect confocal microscope with an infinitesimal pinhole. This assumption, which models only a single magic ray at each scan position, leads to a systematic error between the predicted shape and the experimental data.[17] To remove this systematic error, at each scan position we modeled the confocal microscope as having a finite-sized pinhole and integrated over the associated cone of contributing rays.

Our geometrical-optics-based model, developed to interpret the OPL through thick refractive specimens, can be improved to include the effects of diffraction, nonuniform fringe spacing associated with high-NA objectives,[18] and internal reflections inside the drop. Furthermore, the rich interplay among the contact angle of the drop, the NA of the objective, and the effective pinhole diameter of the microscope suggests that this technique can alternatively be used to calibrate interference microscopes with known refractive samples.

This research was sponsored by an Advanced Technology Development grant from the Microgravity Research Division, NASA. B. Ovryn's e-mail address is ovryn@wave.grc.nasa.gov.

References

1. P. G. de Gennes, Rev. Mod. Phys. **57,** 827 (1985).
2. S. Calixto and M. Ornelas-Rodriquez, Opt. Lett. **24,** 1212 (1999).
3. R. Grunwald, H. Mischke, and W. Rehak, Appl. Opt. **38,** 4117 (1999).
4. B. T. Teipen and D. L. MacFarlane, Appl. Opt. **38,** 2040 (1999).
5. Z. L. Liau, D. W. Nam, and R. G. Waarts, Appl. Opt. **33,** 7371 (1994).
6. E. Sackmann, Science **271,** 43 (1996).
7. G. Wiegand, K. R. Neumaier, and E. Sackmann, Appl. Opt. **37,** 6892 (1998).
8. T. R. Scheuerman, A. K. Camper, and M. A. Hamilton, J. Colloid Interface Sci. **208,** 23 (1998).
9. K. R. Willson and S. Garoff, Colloids Surf. A **89,** 263 (1994).
10. B. Ovryn and J. H. Andrews, ASME, FEDSM97 240-3209 (American Society of Mechanical Engineers, New York, 1997), p. 1.
11. T. Young, Philos. Trans. **95,** 65 (1805).
12. Lord Rayleigh, Proc. R. Soc. London Ser. A **92,** 184 (1915).
13. F. Bashforth and J. C. Adams, *An Attempt to Test the Theories of Capillary Action* (Cambridge U. Press, Cambridge, 1883).
14. P. Concus, J. Fluid Mech. **34,** 481 (1968).
15. The laser feedback interferometer is based on a He–Ne cw laser ($\lambda = 632.8$ nm). The spot size for the 0.8-NA objective is 290 nm, and the sampling step size is 290 nm/pixel. See B. Ovryn and J. H. Andrews, Opt. Lett. **23,** 1078 (1998); Appl. Opt. **38,** 1959 (1999).
16. C. W. Extrand, J. Colloid Interface Sci. **157,** 72 (1993).
17. D. G. Fischer and B. Ovryn, Proc. SPIE **3782,** 378 (1999).
18. C. J. R. Sheppard and K. G. Larkin, Appl. Opt. **34,** 4731 (1995).